Classification of Large-Scale Environments that drive the formation of Mesoscale Convective Systems over Southern West Africa

Francis Nkrumah[1,2], Cornelia Klein[3,5], Kwesi Akumenyi Quagraine[1,4], Rebecca Berkoh Oforiwaa[2,6], Nana Ama Browne Klutse[2,6], Patrick Essien[1,2], Gandomè Mayeul Leger Davy Quenum[2,7] and Hubert Azoda Koffi[6]

[1]Department of Physics, University of Cape Coast, Private Mail Bag, Cape Coast, Ghana;
[2]African Institute of Mathematical Sciences (AIMS), Sector Remera, Kigali 20093, Rwanda;
[3]U.K. Centre for Ecology and Hydrology, Wallingford, United Kingdom
[4]Climate System Analysis Group (CSAG), ENGEO, University of Cape Town, Private Bag X3, Rondebosch, Cape Town 7701, South Africa
[5]Department of Atmospheric and Cryospheric Sciences, University of Innsbruck, Innsbruck, Austria
[6]Department of Physics, University of Ghana, Legon P.O. Box LG 63, Ghana
[7]National Institute of Water (NIW), University of Abomey-Calavi, Godomey, Cotonou 01 PB: 4521, Benin

Correspondence to: Francis Nkrumah (francis.nkrumah@ucc.edu.gh) and Nana Ama Browne Klutse (nklutse@ug.edu.gh)

Abstract. Mesoscale convective systems (MCSs) are frequently observed over southern West Africa (SWA) throughout most of the year. However, it has not yet been identified what variations in typical large-scale environments of the West African monsoon seasonal cycle may favour MCS occurrence in this region. Here, nine distinct synoptic states are identified and are further associated with being either a dry, transition, or monsoon season synoptic circulation type using self organizing maps (SOMs) with inputs from reanalysis data. We identified a pronounced annual cycle of MCS numbers with frequency peaks in April and October that can be associated with the start of rainfall during the major rainy season and the maximum rainfall for the minor rainy season across SWA respectively. Comparing daily MCS frequencies, MCSs are most likely to develop during transition conditions featuring a northward-displaced moisture anomaly (2.8 MCSs per day), which can be linked to strengthened low-level westerlies. Considering that these transition conditions occur predominantly during the pre- and post-monsoon season, these patterns may in some cases be representative of monsoon onset conditions or a delayed monsoon retreat. On the other hand, under monsoon conditions, we observe weakened low-level south-westerlies during MCS days, which reduce moisture content over the Sahel but introduce more moisture over the coast. Finally, we find a majority of MCS-day synoptic states to exhibit positive zonal wind shear anomalies. Seasons with the strongest zonal wind shear anomalies are associated with the strongest low-level temperature anomalies to the north of SWA, highlighting that a warmer Sahel can promote MCS-favourable conditions in SWA. Overall, the SOMS-identified synoptic states converge towards high moisture and high shear conditions on MCS days in SWA, where the frequency at which these conditions occur depends on the synoptic state.

1 Introduction

The region of West Africa is subject to variability in rainfall on both spatial and temporal scales. Fundamentally, the rainfall pattern in West Africa is modulated by the annual change in the position of the Intertropical Convergence Zone (ITCZ) and the West African Monsoon (WAM). Due to endemic poverty, lack of infrastructure and technology, rapid population increase, and significant fluctuation of the WAM, West Africa has been deemed one of the world's most susceptible regions to climate change (IPCC, 2014). The climate of southern West Africa (SWA) can be categorized into four seasonal stages: a dry season from December to February, two wet seasons lasting from April to June, and September to November, and the so-called little dry season in August (e.g. Thorncroft et al. 2011). Between March and June, when low-level winds are more westerly and the intertropical convergence zone (ITCZ) starts to move northward, the precipitable water peaks over SWA (Klein et al. 2021). The ITCZ retreats southward in September, creating the second rainy season, followed by a dry season from November to January.

One major atmospheric disturbance that contributes to the WAM is the presence of Mesoscale Convective Systems (MCSs) which supplies around 30-80 % of the total rainfall during the WAM (Klein et al. 2018). MCSs are organized thunderstorm clusters, often defined to have a minimum horizontal extent of the precipitating area of 100 kilometres in at least one direction (Guo et al. (2022); Chen et al. (2022); Houze (2004)). Maranan et al. (2018) note that diverse MCS sub-groups such as squall- or disturbance lines, structured convective systems, and mesoscale convective complexes impact the hydro-climate of West Africa. In both the tropics and midlatitudes, MCS also

56 contributes significantly to rainfall extremes, rendering them a substantial contributor to the hydrologic cycle (Feng
57 et al. (2021); Li et al. (2020)). More studies have been motivated in recent decades by evaluating drivers that affect
58 rainfall variability and intensity associated with MCSs (Baidu et al. (2022); Augustin et al. (2022)). MCSs, for
59 instance, supply essential precipitation and, as a result, supply water to agriculturally productive regions in the
60 tropics, particularly in semi-arid regions such as the Sahel (Nesbitt et al. (2006)).

61 However, relative to our understanding of MCS drivers in the Sahel, SWA has received less attention. The
62 connections of MCSs to larger-scale atmospheric motion and states are both important and not fully understood for
63 the southern region, hence, a better understanding of large-scale MCS drivers is important for improving
64 precipitation prediction over SWA. Earlier research has suggested an increasing role of other types of less-organized
65 rainfall in place of MCSs over the Guinea Coast (e.g. (Acheampong, 1982; Fink et al., 2006; Kamara, 1986;
66 Omotosho, 1985), with MCS contribution to annual rainfall decreasing from 71% in the Soudanian to 56% in the
67 coastal zone (Maranan et al 2018), emphasizing MCS importance across the SWA region. Maranan et al., 2018 also
68 concluded that precipitable water and Convective Available Potential Energy (CAPE) determine where MCSs may
69 occur in SWA, while zonal wind shear is a stronger predictor for distinguishing between small scattered convection
70 and MCS-type development. Indeed, zonal wind shear intensification was found to be a major driver of increasing
71 frequencies of the most intense Sahelian MCSs over the last three decades (Taylor et al., 2017), a mechanism that
72 was similarly found to play a role for early-season MCS intensification in SWA (Klein et al 2021). Zonal wind
73 shear, which is thought to modulate the storm-available supply of moist buoyant air, is also seen to be very critical
74 to the organization of convective systems (e.g., Alfaro, 2017; Mohr & Thorncroft, 2006). Accordingly, propagating
75 storms with longer-lasting organized precipitation systems were consistently found to be associated with strong
76 vertical wind shear and higher values of CAPE in the Sahel (Hodges & Thorncroft, 1997; Laing et al., 2008; Mohr
77 & Thorncroft, 2006).

78 Previous studies address the large-scale settings for WAM-related rainfall throughout the seasons (Sultan
79 and Janicot, 2003) with less attention given to the importance of large-scale WAM modes and their effect on
80 regional MCS frequencies in SWA. The role of regional MCS-centred environments in the initiation and
81 development of MCSs in West Africa has been well studied (e.g., Klein et al. 2021; Vizy and Cook 2018; Schrage et
82 al. 2006; Maranan et al. 2018). Vizy and Cook (2018) observed that the extension of vertical mixing to the level of
83 free convection, as a result of surface heating, tends to initiate MCSs in an environment where the mid-tropospheric
84 African easterly wave disturbance is located in the east. The vertical wind shear is enhanced as a result of the
85 synoptic disturbance. Klein et al. (2021) suggested that heavy rainfall, due to cold MCSs during both dry and rainy
86 seasons, occurs in an environment with stronger vertical wind shear, increased low-level humidity, and drier mid-
87 levels. Unlike vertical wind shear, Maranan et al., (2018) suggested that thermodynamic conditions such as CAPE
88 and Convective Inhibition (CIN) are of lesser importance for the horizontal growth of convective systems, although
89 they indicate the potential of the initial vertical development of convective systems. Janiga and Thorncroft (2016)
90 also suggested that CAPE, vertical wind shear and column relative humidity are the decisive large-scale
91 environmental parameters that control the characteristics of convective systems. Based on radar and sounding
92 observations aligned around 15ºN, Guy et al. (2011) analyzed MCSs and their respective environmental conditions

over three different regimes of West Africa (maritime, coastal, and continental). They concluded that MCSs tend to occur ahead of the African easterly wave (AEW) trough during the maritime and the continental regime, while they are mostly found behind the trough in the coastal regime.

It is not clear to what extent different large-scale patterns of atmospheric drivers such as temperature, wind, humidity, and CAPE at different stages of the WAM drive the formation of MCSs over SWA. The SWA region differs from its Sahelian counterpart in its closer proximity to the ocean and a distinct bimodal rainfall seasonality. The WAM stages can broadly be classified into a dry season when north-easterly Harmattan winds prevail over most of West Africa during December-February when rainfall mostly occurs off the southern coast of the continent (Thorncroft et al 2011), and the monsoon season from July-September, initiated by a striking jump of the monsoonal rainfall band from coastal regions to the Sahel (Hagos and Cook, 2007). The monsoon months thus represent the unimodal Sahelian rainfall season. In SWA however, the majority of rainfall occurs between the dry months and monsoon months, when the monsoon rainband first passes northward over southern regions from March to June, and subsequently moves southward again when the monsoon retreats in October (e.g. Maranan et al 2018, Klein et al 2021). Here, we define these months when SWA receives most of its rainfall as transition season.

From this SWA perspective, our study systematically classifies the different large-scale patterns across the WAM region and how they are associated with MCSs over SWA. For this purpose, a classification using a self organizing map (SOM; Kohonen 2001) analysis was carried out to characterize large-scale WAM patterns during the 1981-2020 period, which we subsequently grouped into days with MCS occurrence over SWA. The SOM is a clustering technique that is topologically sensitive and uses an unsupervised training method to cluster the training data (Lennard and Hegerl, 2014; Quagraine et al. 2019). This methodology thus allows us to identify favourable types of large-scale environments driving the formation of MCSs within different WAM stages.

The paper is organized as follows: Section 2 details the study area and data sources and how they were processed. In section 3, the SOM methodology and other needed statistics used to investigate the relationship between large-scale environment patterns and particular MCSs are presented. Section 4 discusses the main results, which include the common features and different types of large-scale patterns associated with MCSs. Section 5 provides the summarized conclusions of the study.

2 Data Sources and Processes

2.1 ERA5 Reanalysis Data and MCS Data

The ECMWF fifth-generation atmospheric reanalysis (Hersbach et al., 2020), ERA5, was used as the main data source in this work. The dataset is generated using 41r2 of the Integrated Forecast System (IFS) model, based on a four-dimensional variational data assimilation scheme, and takes advantage of 137 vertical model levels and a horizontal resolution of 0.28125° (31 km). The data provides hourly estimates of model integration. In this study, hourly zonal and meridional winds (650 and 925 hPa), specific humidity (925 hPa), temperature (925 hPa), and convective available potential energy (CAPE) in ERA5 during 1981–2020 were used to explore suitable large-scale

127 environments for the development of MCSs in SWA (5-9ºN, 10ºW-10ºE). The zonal and meridional wind at 925
128 hPa, are used to understand the penetration of monsoon flow inland. The zonal wind difference between 925 hPa
129 and 650 hPa is used as a zonal wind shear change indicator while the temperature at 925 hPa is used to visualize
130 Saharan heat low (SHL) differences. Due to the main direction in which MCSs propagate (east to west), enhanced
131 easterly zonal wind shear are presented as positive anomalies as these are positively related to storm development.
132 Specific humidity (q) at 925 hPa was used to explore whether CAPE changes are controlled by low-level q. We
133 consider also the total column water vapour (TCWV) due to its ability to represent the total gaseous water in the
134 vertical column of the atmosphere which is influenced by the evolution of the humidity field. TCWV represents the
135 precipitable water the atmosphere holds better than the humidity.   The Meteosat Second Generation (MSG)
136 cloud-top temperature data, which are available every 15 minutes from the Eumetsat archives online
137 (https://navigator.eumetsat.int/product/EO:EUM:DAT:MSG:HRSEVIRI) was used in this study. Twelve years of
138 MCS snapshots (2004–15) detected from Meteosat Second Generation 10.8 µm-band brightness temperatures
139 (Schmetz et al., 2002, EUMETSAT 2021) are used to define MCS days in this study. Following (Klein et al., 2021),
140 an MCS is defined here as a -50ºC contiguous cloud area larger than 5000 km2. We consider the MCS images every
141 half hour, for which they are matched up with the half-hourly Integrated Multi-satellite Retrievals for Global
142 Precipitation Measurement (IMERG; Huffman et al. 2019) dataset, using the merged microwave / infra-red
143 ("precipitationCal") rainfall product. An "MCS day" is then defined as a day with at least one hour containing 5
144 simultaneously existing MCSs between 16 and 1900 UTC with maximum rainfall >5mm within the SWA domain.
145 Here, only land-based MCSs because MCSs over land are fundamentally more intense and deep than its counterpart
146 over the ocean (Mohr and Zipser 1996).
147
148 **3 Methodology**
149 **3.1 Self-organising Maps (SOMs) analysis**
150   The study uses the self organizing map (SOM; Kohonen 1982, 2001) from SOM-PAK-3.1 software. The
151 technique is used to identify archetype synoptic circulation patterns over the southern West Africa region by training
152 a 9-node SOM with ERA5 daily mean 925 hPa geopotential height fields to produce 9 characteristic circulation
153 patterns for the period 1981 to 2020. The geopotential height circulation pattern is used here mainly based on its
154 physically realistic output spanning a range of circulation features found in the atmosphere (Hewitson and Crane,
155 2002) and its ability to detect the West African Heat Low (WAHL) which is a key element of the West African
156 monsoon system (Lavaysse et al. 2009; Biasutti et al. 2009). The SOM is mostly the preferred choice over other
157 clustering methods such as the principal component analysis (PCA) or K-means because the data is not discretized
158 and orthogonality is not forced or does not require subjective rotations to produce interpretable patterns. The main
159 advantage of the SOM technique is its ability to deal with non-linear data (such as the continuum of atmospheric
160 conditions) and can easily be visualized and interpreted (Reusch et al. 2005; Lennard and Hegerl, 2014). The steps
161 within the technique can be broadly grouped into two stages, namely the training stage and the mapping stage.
162 Earlier studies (e.g. Hewitson and Crane 2002; Kim and Seo 2016; Lee 2017; Rousi et al. 2015; Sheridan and Lee
163 2012) have successfully used this technique in synoptic climatology to effectively preserve relationships between

164 weather states while giving outputs that are readily understood and can be easily visualized as an array of classified
165 patterns. These classified patterns help in interpreting relationships between large-scale regional circulation patterns
166 and local weather expressions and rainfall extremes (Hewitson and Crane 1996; Cassano et al. 2015; Wolski et al.
167 2018). In this study, the SOM is randomly initialized allowing for hidden patterns and structure in the geopotential
168 height at 925 hPa to be discovered while the algorithm iteratively updates the weights of the nodes to better
169 represent the data. The strength of initializing the SOM this way lies also on its robustness to noise and outliers as a
170 result of the algorithm applying a competitive learning structure to the data which then allows for the formation of
171 distinct clusters. The SOM_PAK algorithm allows the SOM process to minimize quantization and topological errors
172 at the mapping stage when choosing the best SOM as outlined in Lennard and Hegerl (2014). However, there is a
173 trade-off when choosing the size of the SOM, as this is dependent on the need to generalize circulation states for
174 analyses or the need to capture predominant spatial characteristics that affect the local climate. The choice of how
175 many SOM nodes to choose is a trade-off between distinctiveness and robustness. Based on SOM_PAK, we tested
176 node sizes 2x3, 3x3, and 3x4, using the quantization error (QE) as an indicator of the quality and robustness of the
177 respective node size. We find a minimized QE for 3x3 (c.f. Supplementary Figure S1), which, from visual
178 inspection, also shows a larger number of distinct circulation features than 2x3 while producing fewer redundancies
179 than 3x4. Thus, all the following analyses are based on the 3x3 node matrix.
180
3.2 Large-scale WAM patterns on southern West Africa MCS days
182 Based on the 6 different large-scale node patterns, we explore within-node large-scale conditions that
183 characterize MCS days in SWA. For examination of environmental conditions suitable for SWA MCS activity,
184 large-scale conditions were taken from hourly ERA5 reanalysis data sampled at 1200 UTC when the daily
185 convective activity is more representative of pre-convective atmospheric conditions (Klein et al. 2021). Pre-
186 convective conditions are considered in the study to reduce the effects of feedback from the MCSs on environmental
187 conditions (Song et al. 2019). Composites of ERA5 large-scale environmental variables (temperature, wind, specific
188 humidity, and CAPE) are created for all node days, and for MCS days within each SOM node. Finally, the anomaly
189 in large-scale patterns between MCS days and node mean conditions are computed to determine MCS-favourable
190 adjustments in large-scale patterns within each node. A two-sided Student's t-test is used to determine significant
191 differences between node climatologies and MCS-day sub-samples.
192 In addition to large-scale condition composites, we also sample pre-convective (1200 UTC) local
193 atmospheric conditions (ERA5), for each 1800 UTC MCS at the location of minimum cloud top temperature. We
194 only consider 1800 UTC MCSs for local condition sampling to avoid oversampling similar atmospheric states from
195 several MCS time steps. These conditions are compared to the node climatology conditions at the same locations,
196 allowing us to explore the difference in node climatology versus MCS day conditions at the specific locations where
197 MCSs occurred on respective days. Here we only focus on the afternoon peak of convection when it is triggered and
198 is in early stages of organization. It should be noted that driver importance may shift for nocturnal MCSs in later
199 hours, when CAPE is reduced over night and shear may increase further in importance for MCS maintenance (Vizy
200 et al, 2018)

4 Results

4.1 Node seasonality and mean conditions

A 9-node SOM (Fig. 1) with distinct synoptic states was identified, where the nodes are hereafter referred to as nodes one (1) to nine (9). Considering the SOM node frequency distributions in Fig. 1, it is noticeable that the nodes separate different stages of the monsoon circulation seasonality, although certain nodes evidently cover a wider range of months that cannot be represented by the typical monthly grouping of the seasonal cycle (e.g. 2,3,5,8). Circulation patterns in nodes 1, 4, and 7 can be attributed to cases primarily observed in the first three months (January, February, and March) and the last two months (November, and December), hence a pattern most representative of the dry season months. On the other hand, nodes 2, 5, and 8 depict an environment that is prominent during the pre-monsoon and the post-monsoon seasons, with node 2 presenting a clearer seasonal exclusivity during pre-monsoon while nodes 5 and 8 show frequent occurrences during the post-monsoon season. These nodes (nodes 2, 5, and 8) are hence in the following referred to as transition season nodes, a period that connects the dry and monsoon season. The right-hand side of the SOM nodes 3, 6, and 9 represent patterns that cover monsoon season months, but can similarly feature high frequencies outside of the monsoon season (e.g. node 3 with the highest frequency in May).
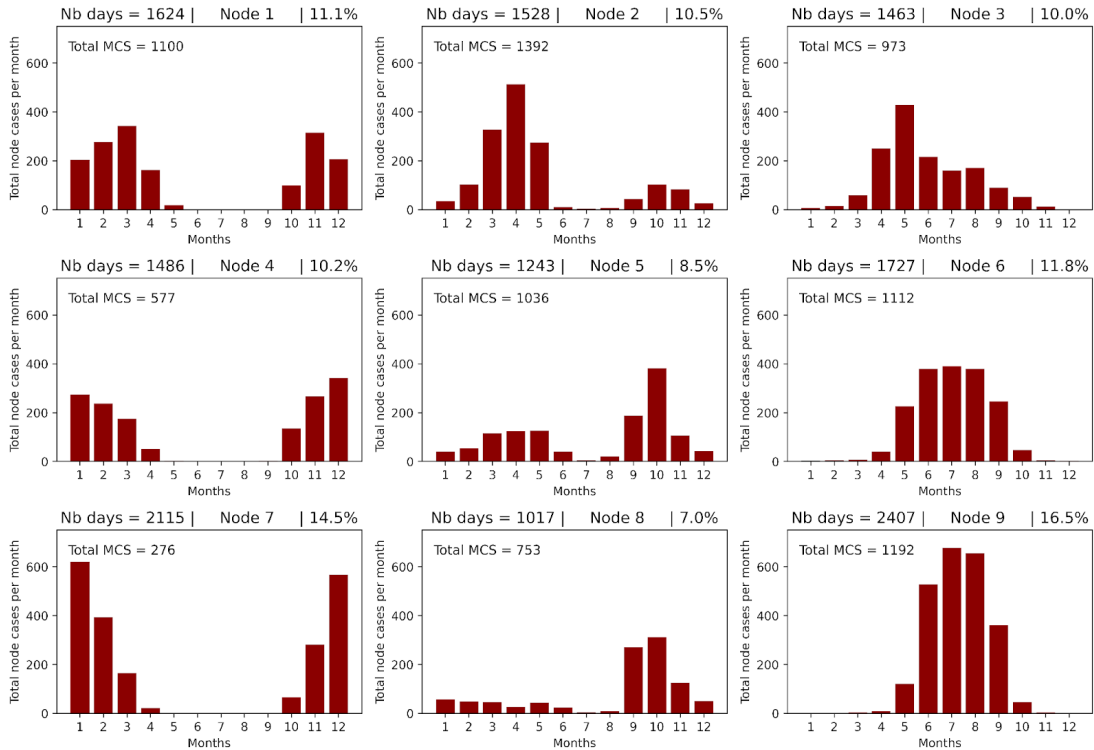
221 **Figure 1.** Monthly distribution of node cases based on SOM analysis. Bar values indicate the total number of MCSs
222 per month from 2004 to 2015. The total number of MCS per node from 2004 to 2015 is displayed in node panels.
223 The title shows the total number of days in each node (left) and the contribution of each node to the total node days
224 (right).

225

226
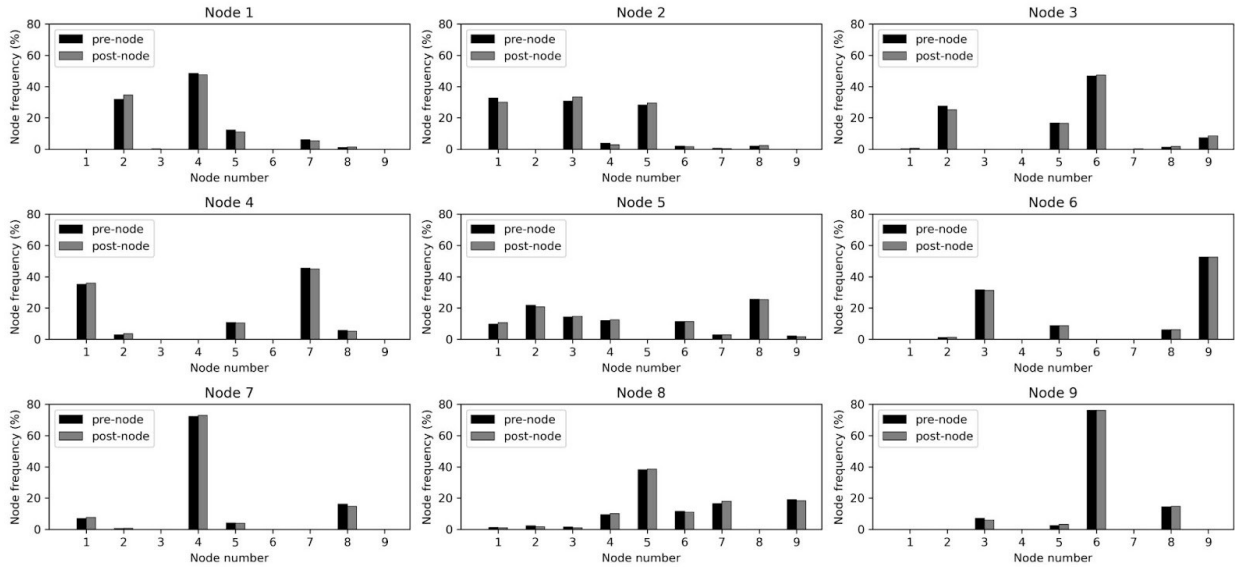
227

228 **Figure 2:** Frequency of nodes (%) preceding (pre-node) or following (post-node) each of the nine nodes.

229

230   To investigate the relationship between nodes across our 3x3 SOM matrix, we now consider the
231 frequencies at which node states are preceded or followed by other nodes in Fig. 2. The resulting frequency
232 distributions reinforce a classification of the matrix columns into dry (1,4,7), transition (2,5,8) and monsoon (3,6,9)
233 season nodes, with the top row (1,2,3) representing nodes that are preceded or followed by nodes of a different
234 season (column) 20-30% of the time. The bottom row nodes (7,8,9) on the other hand are distinct within-season
235 states that are almost never connected to first row nodes (1,2,3) but are reached via intermediate middle row nodes
236 4,5,6. The node matrix separates different season states along rows, while columns seem to represent within-season
237 states where upper and lower rows are separate states, temporally connected by conditions captured by middle-row
238 nodes. Finally, the persistence of nodes presented in Fig. 3 reflects the discussed matrix structure, with connecting
239 middle-row nodes 4,5,6 featuring shortest periods with on average 1.7-1.9 days, suggesting more transient states.
240 Nodes 2,9,7 on the other hand show the smallest number of single day occurrences (consecutive node days = 1),
241 pointing towards more stable, persistent conditions with an average period length of 3.8-4.3 days. Regarding node
242 characteristics, it is striking that each seasonal node group features nodes of differing persistence (c.f. node season
243 order for consecutive node days = 1), rendering node persistence a key difference between same-season nodes in the
244 SOM matrix columns.
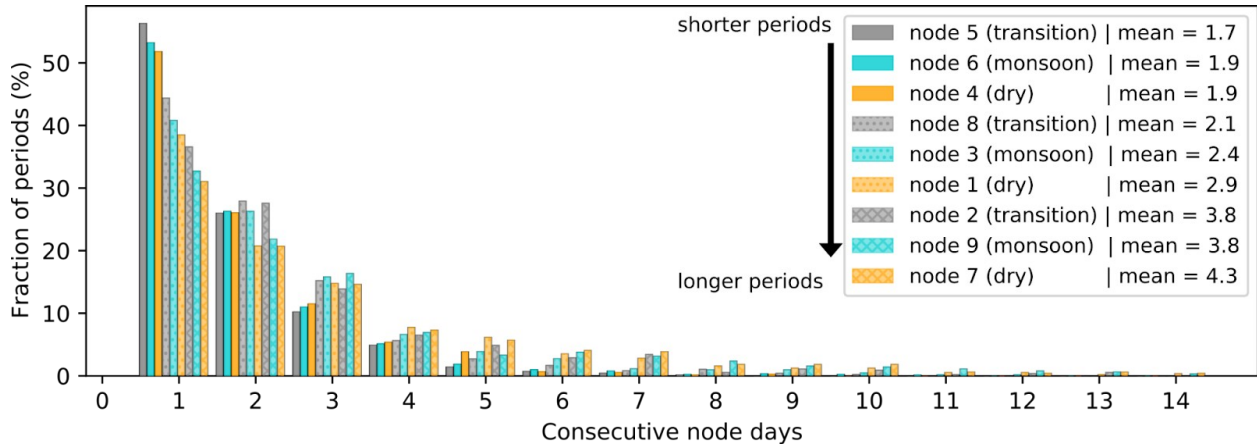
247 **Figure 3:** Fraction of periods covering consecutive days of different lengths per node, with the total percentage for
248 1-14 consecutive node days adding up to 100% per node. The node bars are ordered according to the period fraction
249 for "consecutive node days = 1", revealing the node order going from shorter to longer temporal node persistence, as
250 shown in the legend.

251

252   In the following, we inspect the average atmospheric conditions associated with the identified nodes. The
253 SOM classification of different synoptic states was based on 925 hPa geopotential heights, with resulting patterns
254 shown in Fig. 4. The patterns clearly show the signature of the well-known West African Heat Low (e.g. Lavaysse et
255 al. 2009) moving northwards, strengthening over the course of the annual WAM cycle (from nodes 1, 2, and 3) and
256 peaking in August, evident as an area of low pressure over the Sahara in nodes 3, 6, and 9. Nodes 4, 7, and 8 show
257 stages of the weakening of the heat low, coinciding with a southward movement of the 925 hPa low pressure area.
258 The overlaid 650 hPa wind field reveals mean easterly wind conditions at MCS steering levels across all nodes,
259 suggesting that the dominant propagation direction for MCSs remains east to west for all identified synoptic states.
260
261
262
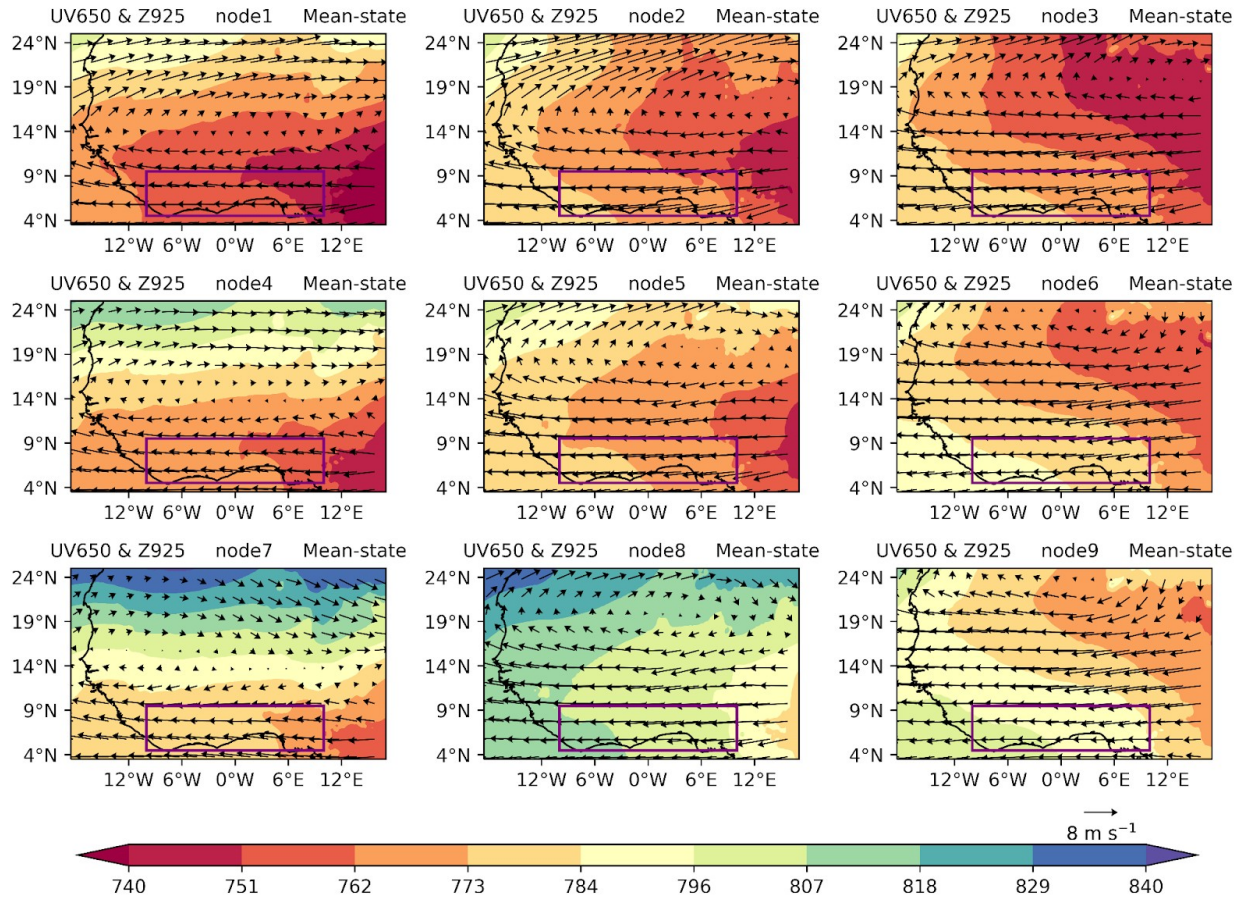
Figure 4. 12 UTC composites of 925-hPa geopotential height (shading; gpm) and 650-hPa winds (vectors; m s^{-1}) in 9 nodes based on SOM analysis. The purple box depicts the SWA region (5º–9ºN, 10ºW–10ºE)

We now examine winds and moisture flows at 925 hPa to explore their behaviour under the nine distinct circulation types identified (Fig. 5). In nodes 1, 4, and 7, the north-easterly winds dominate most of West Africa, with weak southerlies over SWA. This pattern in moisture distribution is evident in the dry season over West Africa, signaling a low moisture presence. The enhanced moisture observed in coastal areas of SWA can be attributed to the penetration of southerly winds. In the transition node 2, the southerly winds strengthen and move inland, causing the north-easterly winds to retreat. A similar effect is observed in nodes 5 and 8 where the north-easterlies become weaker. In nodes 3, 6, and 9, the south-westerlies are intensified and move inland, further enhancing moisture flow from the South Atlantic towards the land, representative of monsoon flow. Wind patterns for mid- and low-levels (Figs. 4 and 5) illustrate vertically-sheared conditions coinciding with regions of high low-level specific humidity in all nodes (purple in Fig. 5), thus marking regions where atmospheric conditions may allow MCS development.
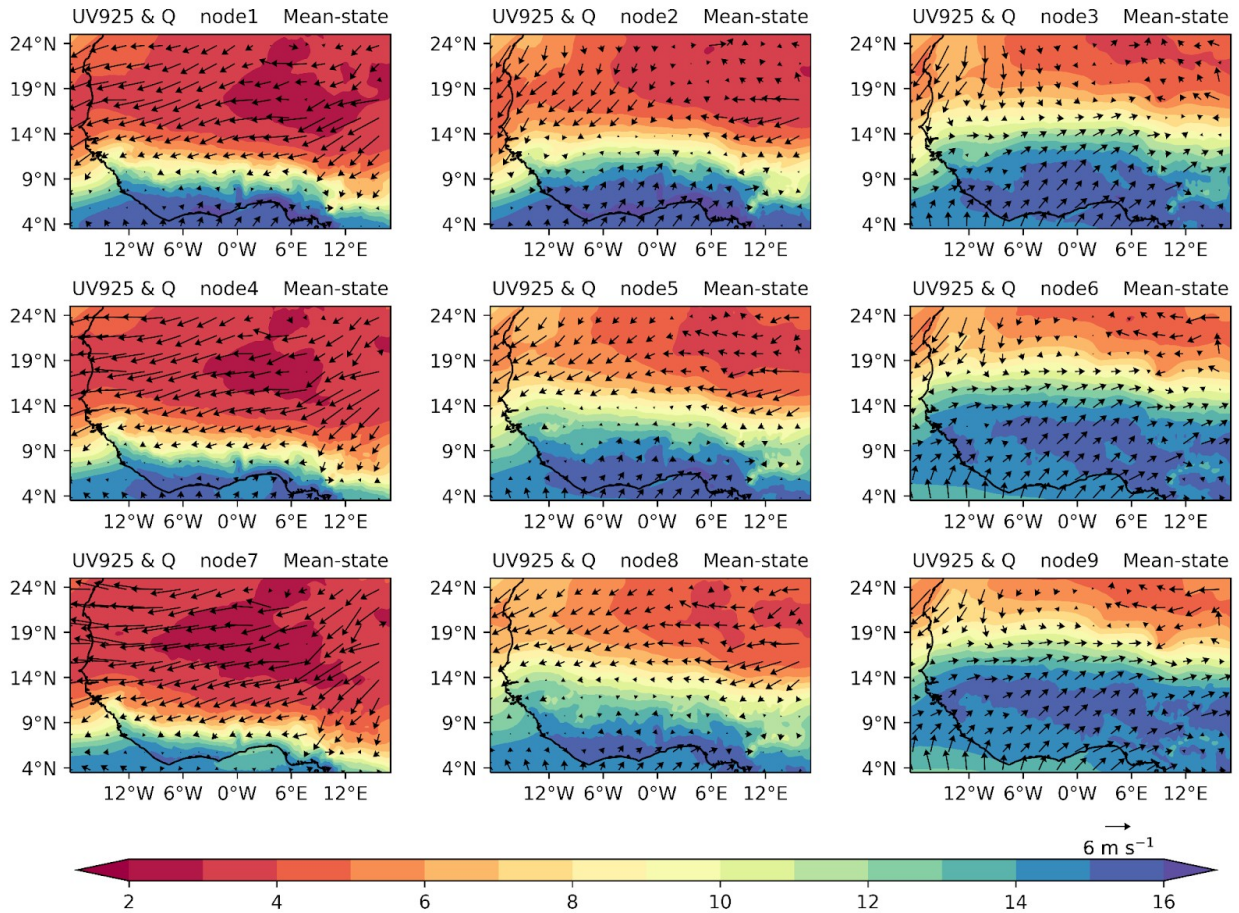
Figure 5. 12 UTC composites of specific humidity (shading; g kg⁻¹) and 925-hPa winds (vectors; m s⁻¹) in 9 nodes based on SOM analysis.

A further investigation was conducted to ascertain the spatial distribution of mean zonal wind shear over SWA (Fig. 6), where easterly shear is represented with a positive sign in this study as it is easterly shear that contributes to MCS development in this region. The patterns in zonal wind shear demonstrate northward transport during the propagation of the WAM cycle and a wider spread of zonal wind shear from first to third column nodes illustrate a strong link of high-shear areas to the propagation of the WAM cycle, and these areas widen as the zonal shear band moves further inland. High-shear areas also closely follow the northern boundary of increased low-level humidity, marking the areas where humidity and shear conditions may allow MCS development. For nodes with high frequency in the monsoon season (nodes 6 and 9), zonal wind shear peaks clearly to the north of the SWA domain. A southward retreat of zonal wind shear is observed during the post-monsoon season (nodes 2, 5, and 8).
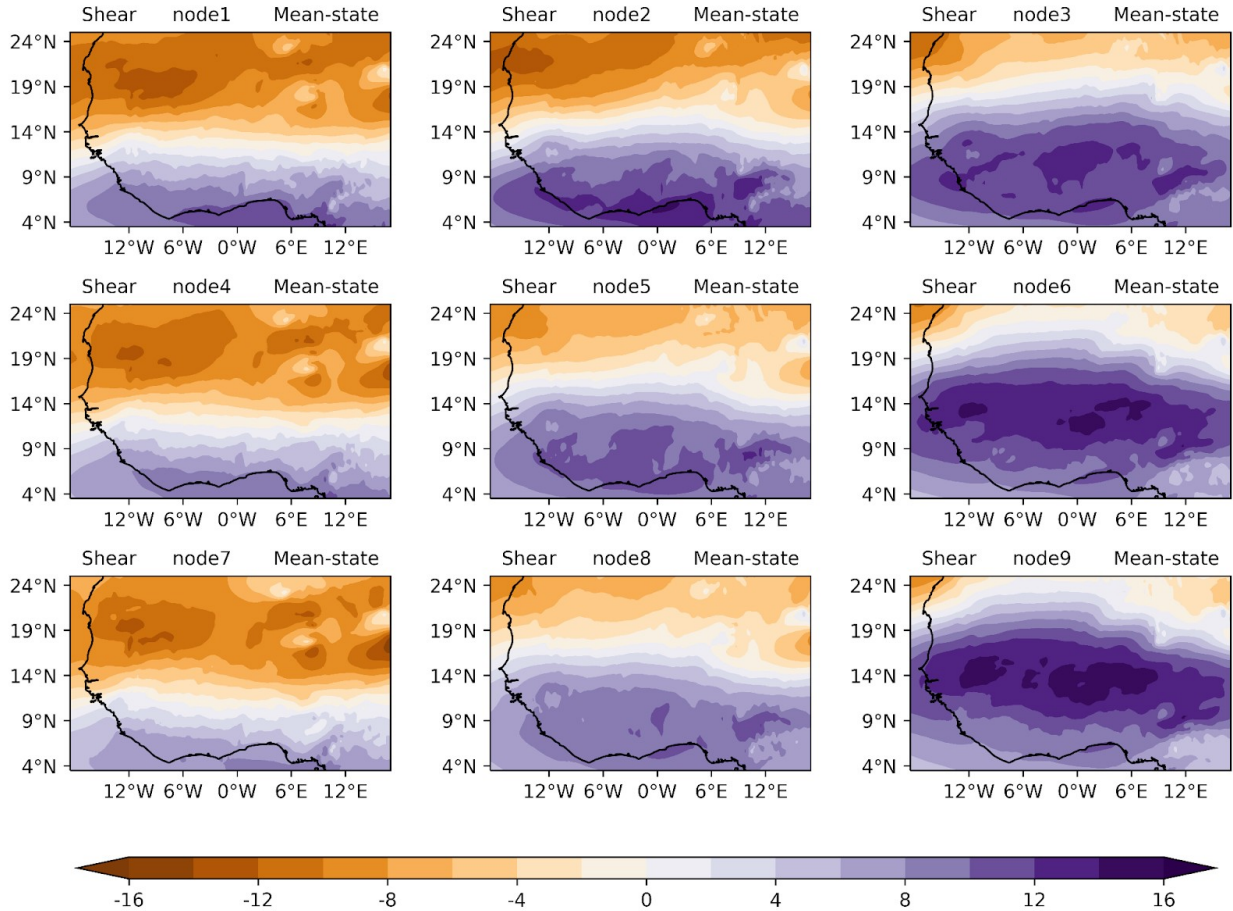
Figure 6. 12 UTC composites of zonal wind shear in 9 nodes based on SOM analysis.

4.2 Large-scale conditions favouring MCS days

The environmental conditions that are associated with MCS occurrence are described in this section. Firstly, the monthly climatology of MCS frequency as captured by our MCS snapshots (average number of MCSs at 1800 UTC across SWA domain) is considered with a focus on rainfall months in Fig. 7, which shows a pronounced annual cycle of MCS numbers with frequency peaks in April and October. These peak months are associated with the start of rainfall during the major rainy season and the maximum rainfall for the minor rainy season across SWA respectively. The monthly climatology of MCS frequency decreases from April to August, with August being the local minimum. This local minimum corresponds to the so-called "little dry season" (Le Barbé et al., 2002; Vollmert et al., 2003) that exists before the southward retreat of the rainbelt.
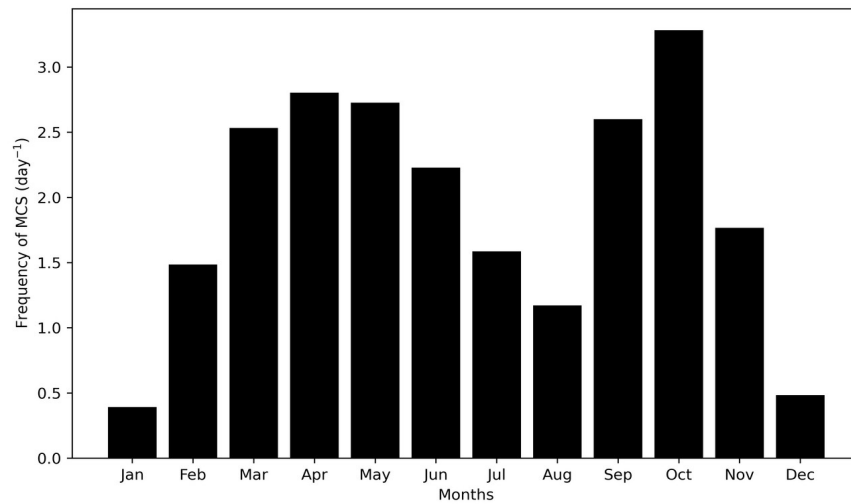
Figure 7. Average annual cycle of MCSs at 1800 UTC within the SWA box showing the monthly average of MCS number per day.

The spatial distribution of MCS frequencies during node days is depicted in Fig. 8. Comparing daily MCS frequencies, we find that MCSs are most likely to develop under transition node (2,5,8) conditions (2.8 MCSs per day) featuring a northward-displaced moisture anomaly (Fig. 9). Given the transition nodes occur predominantly during pre-monsoon (late March to June) and post-monsoon (from September to November) - the major and the minor rainy season respectively in SWA (cf. Fig.~1), these patterns may in some cases be representative of early monsoon onset and a delayed monsoon retreat respectively. MCSs more rarely develop under dry node (1,4,7) conditions, with frequencies as low as 0.6 MCSs per day.
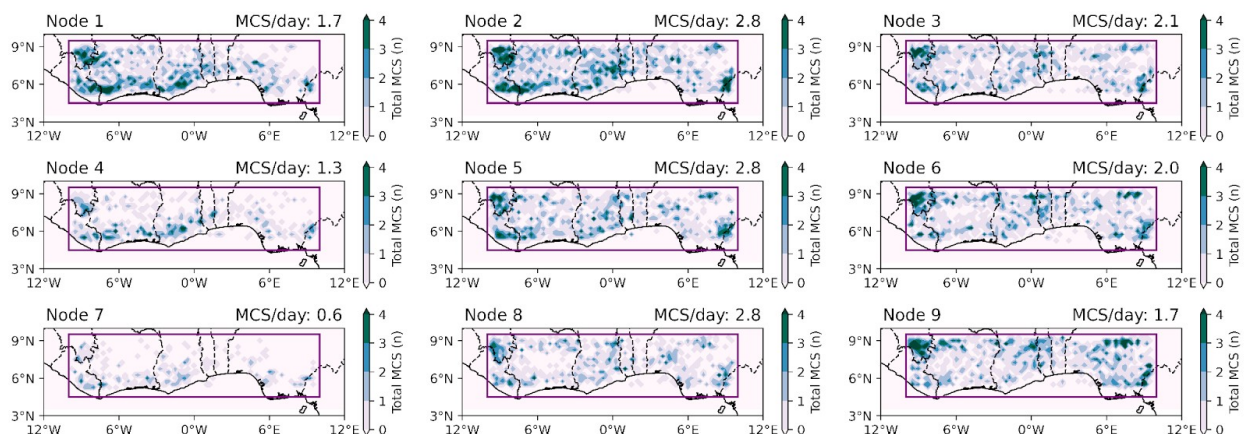
Figure 8. The SWA region indicating the spatial distribution of MCSs during node days. The purple box depicts the main study region of southern West Africa (SWA, 10ºW - 10ºE, 5-9ºN) and titles show the frequency of MCS per day per node within the SWA box.

326
327
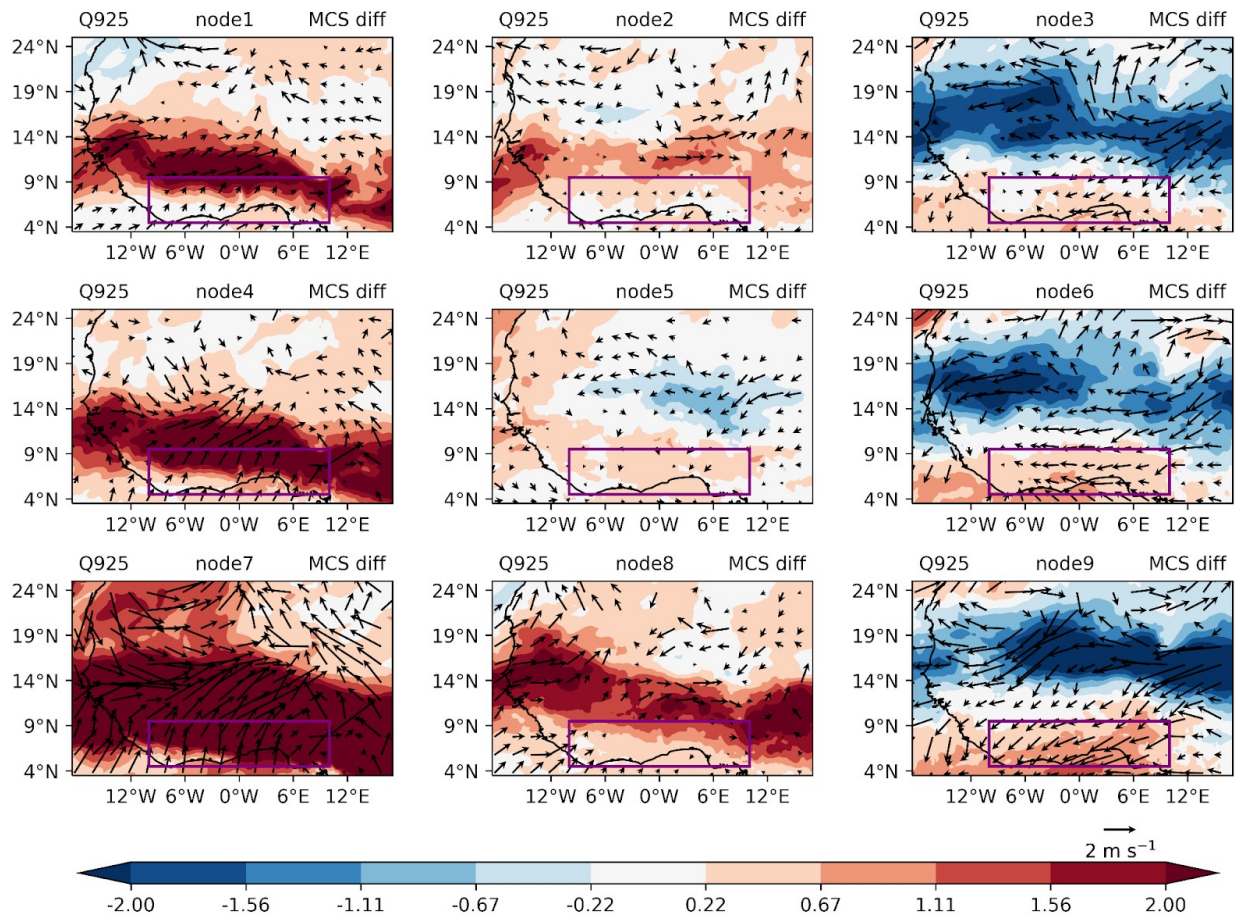
Figure 9. 12 UTC MCS-day composite anomalies of specific humidity (shading; g kg^{-1}) and 925-hPa winds (vectors; m s^{-1}) in 9 nodes based on SOM analysis. Specific humidity anomalies are shown when they are significant at the 5% level; wind vectors are shown when either the zonal or meridional wind anomalies are significant at the 5% level.

During the dry season nodes (1,4,7), a positive widespread moisture anomaly maximum is observed with anomalous south-westerly winds over SWA (Fig. 9). This depicts a substantial enhancement in the low-level moisture transport as a result of the few days with convective activities during the dry season. In the transition nodes (2,5,8), low-level moisture anomalies during convective activity days show weak and mostly insignificant behaviour along the SWA coast based on the two-sided Student's t-test. In node 8, a positive moisture anomaly is located over the northern part of SWA. During monsoon nodes (3,6,9), a notable region of anomalous low-level easterly wind is observed over the Sahel, indicating a weakening of the south-westerly monsoon winds and of the low-level westerly jet, which reduces moisture transport towards the Sahel. This is evident in the negative moisture anomalies over the

Sahel and the increase in moisture over the coastal regions during MCS days, which can result in less convective

activities over the Sahel region and more convective activities over coastal areas.

We now consider low-level temperature anomalies to detect potential changes in temperature gradients and

SHL strength on MCS days. Figure 10 shows a widespread increase in temperature north of SWA during days with

active convection in the dry (1,4,7) and transition (2,8) nodes, which may explain strengthened south-westerly wind

anomalies in some of these nodes (c.f. Fig. 9). The SWA region in the dry and transition nodes, on the other hand,

reveals a negative and/or insignificant change in temperature during MCS days when compared with the mean

climatology. In monsoon nodes 3, 6, and 9, temperatures are enhanced in most parts of West Africa including SWA

during days with active convection.
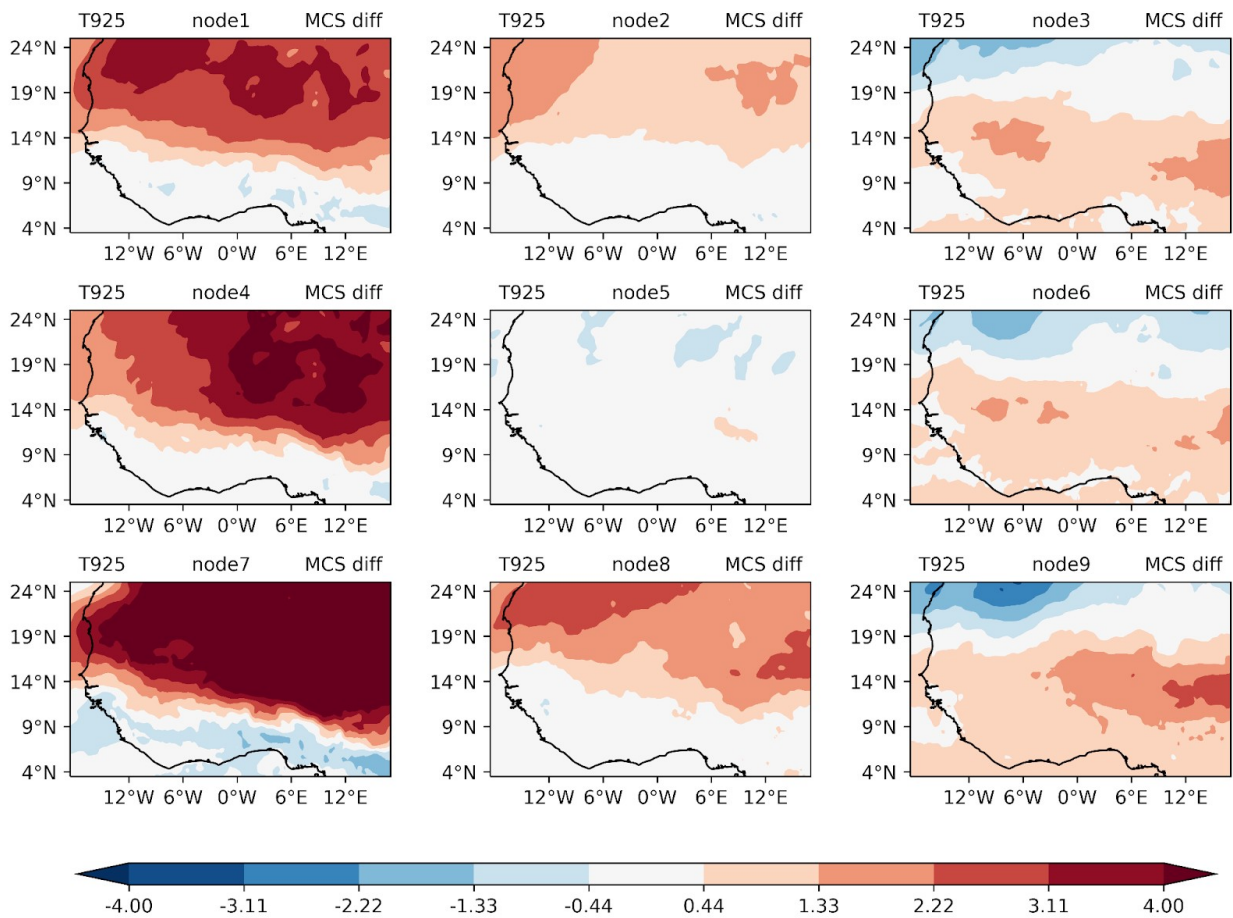
Figure 10. 12 UTC composite anomalies of 925hPa temperatures (℃) in 9 nodes based on SOM analysis. Temperature anomalies are shown when they are significant at the 5% level.

Figure 11 shows the spatial distribution of zonal wind shear anomaly between days with convective MCSs

over SWA and the climatological zonal wind shear mean for the 9 different nodes across West Africa. Generally, all

dry and transition nodes except node 5, reveal a widespread increase in zonal wind shear anomaly over West Africa with the dry nodes depicting stronger events. Zonal wind shear anomalies tend to be stronger during the dry season with their peak partly over SWA, but resides to the north of SWA during the transition seasons (nodes 2 and 8). The positive shear anomaly patterns align with patterns of strengthened temperature gradients for respective dry and transition season nodes (c.f. Fig. 10): only node 5 shows no large-scale temperature anomalies and consequently patchy changes in shear, while strongest shear increases occur for node 7 alongside the highest temperature gradient increase. Nodes 2 and 8 experience an appreciably significant increase in zonal wind shear over SWA for MCS days during the transition seasons. The monsoon nodes (3,6,9), on the other hand, exhibit a significant increase in zonal wind shear mainly confined to the south with a pronounced signal in node 9 associated with a peak in eastern-Sahel warming (Fig. 10). In line with the expected zonal wind shear response to an increased large-scale meridional temperature gradient, we thus find the strongest zonal wind shear anomalies for nodes with strongest positive low-level temperature anomalies to the north of SWA (nodes 1,4,7; followed by nodes 2,8), highlighting that a warmer Sahel can promote MCS-favourable shear conditions in SWA.
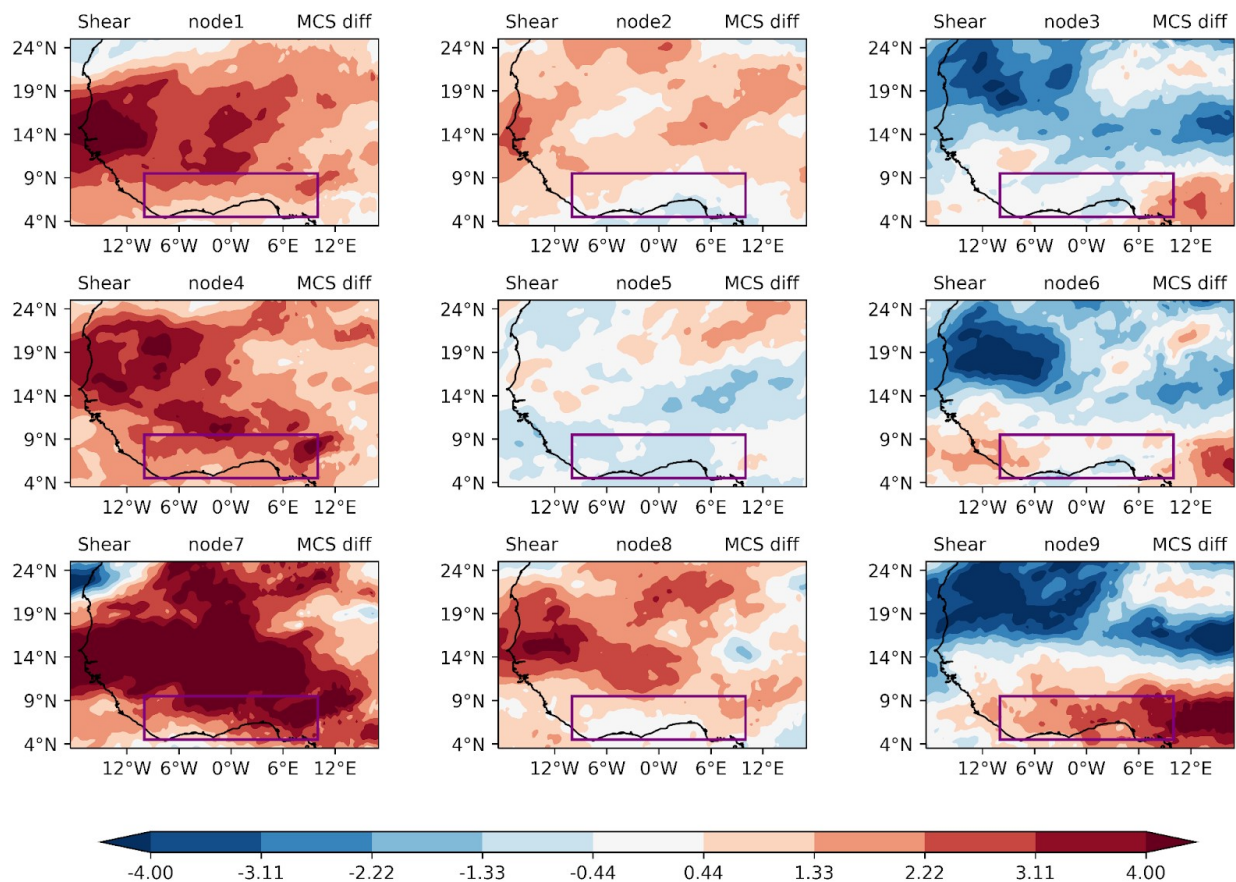
Figure 11. 12 UTC composite anomalies of zonal wind shear (m s^{-1}) in 9 nodes based on SOM analysis. zonal wind shear anomalies are shown when they are significant at the 5% level.

16   16

378   Investigating the first-order condition for convection development, we also evaluate CAPE for a parcel at
379 925 hPa to ascertain the level of increased MCS-day instability in various nodes over SWA (Fig. 12). A large strip
380 of higher CAPE values extending over the entire region of SWA and the southern Sahel from 5°N−15°N is observed
381 (dry and transition nodes). This large strip of higher CAPE is situated mainly in central and east of SWA, while part
382 of the west coast tends to depict patterns of lower CAPE values, suggesting increased MCS likelihood only for the
383 central and eastern parts of the domain. During monsoon nodes, node 3 shows a swath of high CAPE values in
384 particular to the coast and in some instances extends to the entire SWA (node 6) and north of SWA (node 9). Higher
385 CAPE conditions over SWA are to differing degrees significantly associated with decreased CAPE in the Sahelian
386 region, creating a dipole pattern that can occur during transition and monsoon periods according to node frequencies
387 (cf. Fig 1). Overall, all nodes show positive CAPE and negative convective inhibition (c.f. Supplementary Fig. S4)
388 anomalies for MCS days in parts of SWA, creating an environment sufficiently unstable to support the development
389 of convection. The close alignment with regions of increased low-level humidity (Fig. 9) suggests increased low-
390 level moisture advection as the main driver for these instability changes.

391

392
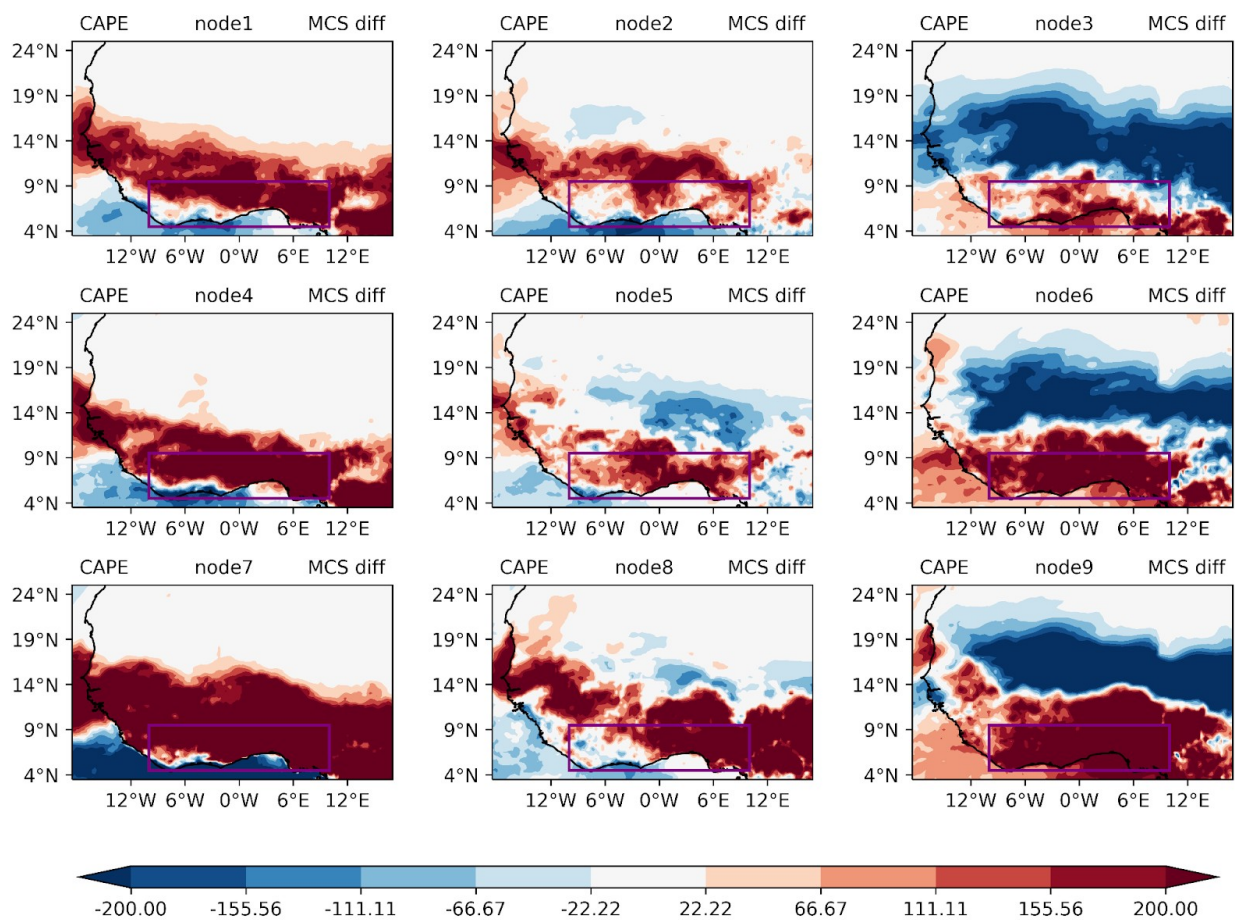
Figure 12. 12 UTC composite anomalies of CAPE (J kg^{-1}) for MCSs occurring in each type of large-scale
394 environment determined by the SOM analysis over SWA. CAPE anomalies are shown when they are significant at
395 the 5% level.

4.3 MCS driver variability within nodes

The drivers of MCSs within different nodes are considered to examine their relative importance within the different large-scale states (Fig. 13), concentrating on total column water vapor (TCWV) and zonal wind shear. TCWV instead of single-level specific humidity is used here to capture the changes in total moisture available to MCSs under the different regimes. For this analysis, both atmospheric drivers were sampled locally under pre-convective conditions at 1200 UTC at the location where MCSs occurred subsequently at 1800 UTC. Dry season nodes (1,4,7) exhibit the lowest climatological conditions in both wind shear and TCWV. This illustrates the relatively hostile conditions for storms in the mean for these nodes, predominantly representing dry season conditions and explaining the low storm frequency of only 0.6-1.7 MCSs per day (cf. Fig. 9). All monsoon nodes (3,6,9) show on average slightly higher TCWV than transition nodes (2,5,8), but covering a similar range of shear conditions. Considering MCS day conditions, most nodes feature significantly higher TCWV and shear conditions relative to the climatological mean node states. Solely for monsoon season nodes (3,6,9), TCWV shows no significant change, while shear still increases for nodes 6 and 9. Interestingly, for MCS days, dry season node conditions even move into the ranges of climatological conditions identified for transition season nodes, though still exhibit the lowest values in TCWV and zonal wind shear compared to MCS day conditions of transition and monsoon season nodes.
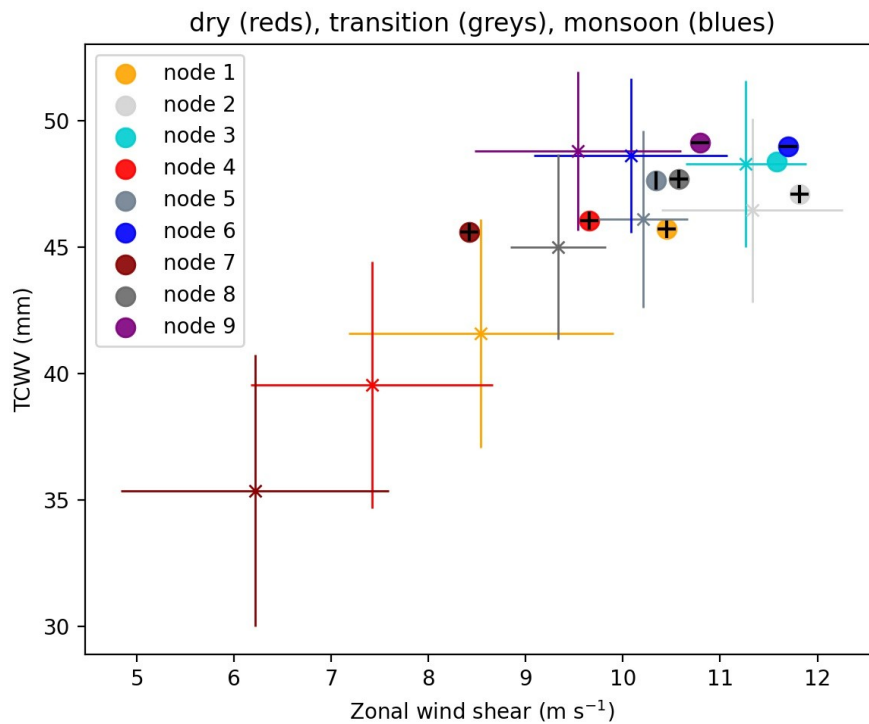
Figure 13. Mean node climatologies and MCS-day conditions over SWA. The node climatologies are depicted as (x) with whiskers extending one standard deviation. Circles denote corresponding mean MCS-day conditions.

432 Horizontal black lines in the circles indicate significant differences in the shear mean, while a vertical black line
433 marks a significant difference in the TCWV mean against node climatologies based on Welch's t-tests ($p < 0.05$)
434
435

436   Generally, it can be noted that all nodes show increased TCWV on MCS days compared to their
437 climatology. The smallest changes for both TCWV and zonal wind shear between climatology and MCS day occur
438 for node 3, which has its highest frequency for pre-monsoon transition month May but is still common throughout
439 the monsoon season (c.f. Fig. 1) . Together with node 5, it is also the only node for which zonal wind shear
440 conditions remain approximately similar, but with climatological zonal wind shear strengths already reaching > 10
441 m/s at MCS location. Overall, mean node environmental conditions become more similar for MCS-days relative to
442 the climatologies, illustrating that favourable MCS conditions converge towards high TCWV and high zonal wind
443 shear environments irrespective of the large-scale situation.

444 **5 Conclusion**

445   In this study, we identified nine synoptic states over West Africa and examined what changes are
446 associated with favourable MCS environments in Southern West Africa under these states. For the definition of
447 synoptic states and MCS days, we used self-organizing maps (SOM) based on ERA5 925 hPa geopotential height
448 data and 12 years of MCS imagery using Meteosat Second Generation (MSG) 10.8 μm-band brightness temperature
449 data (2004-15), respectively. To investigate how the distinct synoptic states change to support MCS development in
450 SWA, we compared mean climatological node states to node sub-samples of MCS days in SWA.
451 We found the identified synoptic states, based on a 3x3 SOM matrix, to exhibit frequency distributions that are
452 linked to different phases of the West African seasonal rainfall cycle, which we classified as dry (nodes 1, 4, 7),
453 transition (nodes 2, 5, 8) and monsoon (nodes 3, 6, 9) season, albeit most nodes are not strictly confined to one
454 season. We found that different nodes identified within one season exhibit key differences in persistence
455 (consecutive node days) and node succession. Specifically, each season (dry, transition, monsoon) contains a node
456 that is frequently preceded or followed by a node of another season (nodes 1, 2, 3), as well as a node that
457 predominantly shows within-season succession (nodes 7, 8, 9). The shortest node persistence of 1.7-1.9 days was
458 found for nodes 4, 5, and 6. These nodes at the same time represent intermediate synoptic states that develop from or
459 into a different node of the same season. The SOM methodology thus seems a promising approach to identify states
460 of variability beyond the established West African monsoon phases (e.g. Thorncroft et al 2011).
461   In spite of these clear differences in node persistence and succession, large-scale differences in node
462 climatologies of atmospheric MCS drivers (low-level wind field, 925hPa humidity, and temperature, CAPE) are
463 most pronounced between nodes of different seasons, while same-season nodes show strong pattern similarities.
464 Notably, however, MCS-day node anomalies, as compared to full node climatologies, all show clear increases in
465 low-level humidity and/or wind shear over the SWA region, which are important ingredients for MCS development
466 (Klein et al. 2021). For dry season nodes, these changes are associated with higher temperatures in the Sahel and
467 Sahara, driving stronger south-westerly humid winds inland while increasing shear due to an enhanced meridional

19   19

468 temperature gradient on land. Monsoon season nodes on the other hand show the opposite, where a weakening of the

469 south-westerlies and of the Sahelian low-level westerly jet indicates a south-ward shift of the monsoon circulation.

470 This results in more moisture, and for nodes 6, 9 also in higher shear, over SWA, where the latter is linked to a

471 warmer and presumably drier Sahel during monsoonal southward shifts, creating a dipole pattern. Generally, we find

472 the strongest MCS-day zonal wind shear anomalies over SWA for nodes with the strongest low-level temperature

473 anomalies to the north of SWA, representative of favorable MCS conditions in SWA during periods of a warmer

474 Sahel. Strengthened wind shear due to a warmer Sahara was previously also identified to drive MCS intensification

475 in the Sahel (Taylor et al. 2017).

476 Thus, meridional displacements of the extent to which south-westerly winds from the Atlantic penetrate

477 inland and the associated positioning of the meridional temperature gradient seems to be key mechanisms by which

478 MCS days in SWA are created for both, dry and monsoon season node synoptic states. Such meridional

479 displacements have previously been identified as important drivers of monsoon variability on inter-annual (e.g.

480 Nicholson and Webster 2008) and intra-seasonal (e.g. Janicot et al. 2011, Talib et al. 2022) timescales. Here, we are

481 looking at higher-frequency changes with average node persistence between 1.7-4.3 days. Transition nodes show

482 weaker signals and a mixture of a southward (node 5) or northward (node 8) displaced circulation, which may be

483 linked to the fact that these nodes predominantly occur in months when the monsoon circulation and its rainfall band

484 are positioned over SWA (Maranan et al. 2018). Indeed, we find MCSs to be most likely to develop under transition

485 season node conditions (2.8 MCS/day across SWA domain). There is strong potential for further exploration of the

486 synoptic differences between transition season nodes and their meridional shifts on MCS days, as these may in some

487 cases be representative of monsoon onset conditions or a delayed monsoon retreat.

488 Pre-convective atmospheric anomalies at locations where afternoon development of MCSs took place were

489 found to be weakest for transition season node 5, lacking significant changes in wind shear, and for monsoon season

490 nodes 3, 6, 9, for which none showed significant changes in total column moisture, albeit increased moisture at low-

491 levels contributes to elevated CAPE. Here it should be noted that weak anomalies signify nodes whose mean

492 climatological conditions already tend to be more favorable for MCS development with respect to that variable, such

493 that MCS days differ little from the node mean, which, perhaps expectedly, is the case for certain transition and

494 monsoon rather than dry season nodes.

495 Generally, however, we find node environmental conditions to become more similar for MCS days relative

496 to their node climatologies, illustrating that favorable MCS conditions converge towards high TCWV/high zonal

497 wind shear states. Overall, our results show that MCSs develop on average in high moisture, high zonal wind shear

498 local environments under all large-scale situations throughout the year. The large-scale situation however defines the

499 frequency at which favorable MCS environments can occur.

500

501 *Code and data availability*. Codes for the findings of this study are available upon reasonable request from the

502 authors. The processing of ERA5 data made direct access to the primary data archive held at ECMWF, and is

503 available from the Copernicus Data Store (https://cds.climate.copernicus.eu/) and the MSG data are available from

504 http://www.eumetsat.int.

505

506 *Author contributions*. FN, NABK and CK conceptualized the study, with input from KAQ; All authors contributed
507 to and discussed the methodological design, and analyses were conducted by FN and CK; FN, ROB and KAQ wrote
508 the manuscript draft; CK, NABK, PE, GMLDQ and HAK reviewed and edited the manuscript.
509

510 *Competing interests*. The contact author has declared that none of the authors has any competing interests.

511 *Acknowledgments.* This work is supported by a grant from the Government of Canada, provided through Global
512 Affairs Canada, www.international.gc.ca (accessed on 1 January 2021), and the International Development Research
513 Centre, www.idrc.ca, (accessed on 1 June 2022) to the African Institute for Mathematical Sciences—Next Einstein
514 Initiative (AIMS-NEI) [Number: 108246-001]. CK acknowledges funding from the NERC-funded LMCS project
515 (NE/W001888/1). KQ also acknowledges funding from the National Research Foundation (NRF), South Africa.

516 **References**

517 Alfaro, D. A.: Low-Tropospheric Shear in the Structure of Squall Lines: Impacts on Latent Heating under Layer-
518   Lifting Ascent, J Atmos Sci., 74, 229–48, https://doi.org/10.1175/JAS-D-16-0168.1, 2017.

519 Augustin, D., Pascal, I.M., Jores, T.K., Elisabeth, F.D., Cesar, M.B., Michael, T.F., Roméo-Ledoux, D.T.,
520   Marceline, M., Gladys, K.N.F. and Firmin, B.A.: Impact Assessment of the West African Monsoon on
521   Convective Precipitations over the Far North Region of Cameroon, Adv. Space Res.,
522   https://doi.org/10.1016/j.asr.2022.04.044, 2022.

523 Baidu, M., Schwendike, J., Marsham, J.H. and Bain, C.: Effects of Vertical Wind Shear on Intensities of Mesoscale
524   Convective Systems over West and Central Africa, Atmos. Sci. Lett, e1094, https://doi.org/10.1002/asl.1094,
525   2022.

526 Biasutti, M., Sobel, A. H., & Camargo, S. J.: The role of the Sahara low in summertime Sahel rainfall variability and
527   change in the CMIP3 models. Journal of Climate, 22(21), 5755-5771,
528   https://doi.org/10.1175/2009JCLI2969.1, 2009.

529 Cassano, E.N., Glisan, J.M., Cassano, J.J., Gutowski Jr, W.J. and Seefeldt, M.W.: Self-Organizing Map Analysis of
530   Widespread Temperature Extremes in Alaska and Canada, Clim. Res. 62, 199-218,
531   https://doi.org/10.3354/cr01274, 2015.

532 Chen, Y., Luo, Y. and Liu, B.: General Features and Synoptic-Scale Environments of Mesoscale Convective
533   Systems over South China during the 2013-2017 Pre-Summer Rainy Seasons, Atmos. Res., 266,
534   https://doi.org/10.1016/j.atmosres.2021.105954, 2022.

535 Feng, Z., Leung, L.R., Liu, N., Wang, J., Houze Jr, R.A., Li, J., Hardin, J.C., Chen, D. and Guo, J. A.: Global High-
536   Resolution Mesoscale Convective System Database Using Satellite-Derived Cloud Tops, Surface
537   Precipitation, and Tracking, J. Geophys. Res. Atmos. 126, e2020JD034202,
538   https://doi.org/10.1029/2020JD034202, 2021.

539 Guo, Y., Du, Y., Lu, R., Feng, X., Li, J., Zhang, Y. and Mai, Z.: The Characteristics of Mesoscale Convective
540   Systems Generated over the Yunnan-Guizhou Plateau during the Warm Seasons, Int. J. Climatol.,
541   http://doi.org/10.1002/joc.7647, 2022.

542 Guy, N., Rutledge, S.A. and Cifelli, R.: "Radar Characteristics of Continental, Coastal, and Maritime Convection
543   Observed during AMMA/NAMMA", Q. J. R. Meteorol. Soc. 137, 1241-56, http://doi.org/10.1002/qj.839,
544   2011.

545 Hagos, S. M. and Cook, K. H.: Dynamics of the West African Monsoon Jump, J. Clim., 20(21), 5264–5284,
546   https://doi:10.1175/2007JCLI1533.1, 2007.

547 Hewitson, B. C., & Crane, R. G.: Climate Downscaling: Techniques and Application. Clim. Res. 7, 85-95,
548   https://doi.org/10.3354/cr007085, 1996.

549 Hewitson, B. C., & Crane, R. G. "Self-Organizing Maps: Applications to Synoptic Climatology." Clim. Res. 22, 13-
550   26, https://doi:10.3354/cr022013, 2002.

551 Hodges, K.I. and Thorncroft, C.D.: Distribution and Statistics of African Mesoscale Convective Weather Systems
552   Based on the ISCCP Meteosat Imagery, Mon Weather Rev 125, 2821-37, https://doi.org/10.1175/1520-
553   0493(1997)125<2821:DASOAM>2.0.CO;2, 1997.

554 Houze Jr, Robert A.: Mesoscale Convective Systems", Rev. Geophys., 42, http://doi:10.1029/ 2004RG000150,
555   2004.

556 Hussain, M.S., Kim, S. and Lee, S.: On the Relationship between Indian Ocean Dipole Events and the Precipitation
557   of Pakistan, Theor. Appl. Climatol. 130, 673-85, http://doi.org/10.1007/s00704-016-1902-y, 2017.

558 IPCC: Climate Change, 2014: Synthesis Report. Contribution of Working groups I, II, and III to the Fifth
559   Assessment Report of the Intergovernmental Panel on Climate Change [Core Working Team, R.K. Pachauri
560   and L.A. Meyer (eds)]. IPCC, Geneva, Switzerland, 151, 2014

561 Janicot, S., Caniaux, G., Chauvin, F., De Coëtlogon, G., Fontaine, B., Hall, N., Kiladis, G., Lafore, J.-P., Lavaysse,
562   C., Lavender, S.L., Leroux, S., Marteau, R., Mounier, F., Philippon, N., Roehrig, R., Sultan, B. and Taylor,
563   C.M.: Intraseasonal variability of the West African monsoon. Atmospheric Science Letters, 12, 58–66,
564   https://doi.org/10.1002/asl.280, 2011

565 Janiga, M.A. and Thorncroft, C.D.: The Influence of African Easterly Waves on Convection over Tropical Africa
566   and the East Atlantic, Mon Weather Rev 144, 171-92, https://doi.org/10.1175/MWR-D-14-00419.1, 2016.

567 Kamara, S. I.: The Origins and Types of Rainfall in West Africa, Weather 41, 48-56, https://doi.org/10.1002/j.1477-
568   8696.1986.tb03787.x, 1986.

569 Kim, H.K. and Seo, K.H.: Cluster Analysis of Tropical Cyclone Tracks over the Western North Pacific Using a Self-
570   Organizing Map, JCLI 29, 3731-51, https://doi.org/10.1175/JCLI-D-15-0380.1, 2016.

571 Klein, C., Belušić, D., & Taylor, C. M.: Wavelet scale analysis of mesoscale convective systems for detecting deep
572   convection from infrared imagery.Journal of Geophysical Research: Atmospheres, 123, 3035 - 3050.
573   https://doi.org/10.1002/2017JD027432, 2018.

574 Klein, C., Nkrumah, F., Taylor, C.M. and Adefisan, E.A.: Seasonality and Trends of Drivers of Mesoscale
575   Convective Systems in Southern West Africa, JCLI 34, 71-87, https://doi.org/10.1175/JCLI-D-20-0194.1,
576   2021.

577   Kohonen, T. "Self-Organizing Maps.-Springer Series in Information Sciences, V. 30, Springer Sci. Rev.,
578   https://doi.org/10.1007/978-3-642-56927-2, 2001.

579   Kusangaya, S., Warburton, M.L., Van Garderen, E.A. and Jewitt, G.P.: Impacts of Climate Change on Water
580   Resources in Southern Africa: A Review, Phys. Chem. Earth., 47-54,
581   https://doi.org/10.1016/j.pce.2013.09.014, 2014.

582   Laing, A.G., Carbone, R., Levizzani, V. and Tuttle, J.: The Propagation and Diurnal Cycles of Deep Convection in
583   Northern Tropical Africa, Q J R Meteorol Soc. 134, 93-109, http://doi.org/10.1002/qj.194, 2008.

584   Lavaysse, C., Flamant, C., Janicot, S., Parker, D.J., Lafore, J.P., Sultan, B. and Pelon, J.: Seasonal Evolution of the
585   West African Heat Low: A Climatological Perspective, Clim. Dyn. 33, 313-30,
586   https://doi.org/10.1007/s00382-009-0553-4, 2009.

587   Le Barbé, L., Lebel, T., & Tapsoba, D.: Rainfall variability in West Africa during the years 1950 - 90. J. Clim.
588   15(2), 187-202, https://doi.org/10.1175/1520-0442(2002)015<0187:RVIWAD>2.0. CO;2, 2002.

589   Li, P., Moseley, C., Prein, A.F., Chen, H., Li, J., Furtado, K. and Zhou, T.: Mesoscale Convective System
590   Precipitation Characteristics over East Asia. Part I: Regional Differences and Seasonal Variations, J. Clim.
591   33, 9271-86, https://doi.org/10.1175/JCLI-D-20-0072.1, 2020.

592   Maranan, M., Fink, A.H. and Knippertz, P.: Rainfall Types over Southern West Africa: Objective Identification,
593   Climatology and Synoptic Environment, Q J R Meteorol Soc. 144, 1628-48, https://doi.org/10.1002/qj.3345,
594   2018.

595   Mohr, K. I., and Zipser, E. J.: Mesoscale convective systems defined by their 85-GHz ice scattering signature: Size
596   and intensity comparison over tropical oceans and continents. *Mon. Wea. Rev.*, 124, 2417-2437,
597   https://doi:10.1175/1520-0493(1996)124<2417:MCSDBT>2.0.CO;2, 1996

598   Mohr, K.I. and Thorncroft, C.D.: Intense Convective Systems in West Africa and Their Relationship to the African
599   Easterly Jet, Q J R Meteorol Soc. 132, 163-76, https://doi.org/10.1256/qj.05.55, 2006.

600   Nesbitt, S.W., Cifelli, R. and Rutledge, S.A.: Storm Morphology and Rainfall Characteristics of TRMM
601   Precipitation Features, Mon Weather Rev 134, 2702-21, https://doi.org/10.1175/MWR3200.1, 2006.

602   Nicholson, S. E. and Webster, P. J.: A physical basis for the interannual variability of rainfall in the Sahel, Q. J. R.
603   Meteorol. Soc., 2084 (November), 2065–2084, doi:10.1002/qj, 2008.

604   Queralt, S., Hernández, E., Barriopedro, D., Gallego, D., Ribera, P. and Casanova, C.: North Atlantic Oscillation
605   Influence and Weather Types Associated with Winter Total and Extreme Precipitation Events in Spain,
606   Atmos. Res. 94, 675-83, https://doi.org/10.1016/j.atmosres.2009. 09.005, 2009.

607   Schmetz, J., Pili, P., Tjemkes, S., Just, D., Kerkmann, J., Rota, S. and Ratier, A.: An Introduction to Meteosat
608   Second Generation (MSG)", Bull Am Meteorol Soc 83, 977-92, https://doi.org/10.1175/1520-
609   0477(2002)083<0977:AITMSG>2.3.CO;2, 2002.

610   Schrage, J.M., Fink, A.H., Ermert, V. and Ahlonsou, E.D.: Three MCS Cases Occurring in Different Synoptic
611   Environments in the Sub-Sahelian Wet Zone during the 2002 West African Monsoon, J Atmos Sci 63, 2369-
612   82, https://doi.org/10.1175/JAS3757.1, 2006.

613   Sheridan, S. and Lee, C.C.: Synoptic Climatology and the Analysis of Atmospheric Teleconnections, Prog Phys
614   Geogr. 36, 548-57, https://doi.org/10.1177/0309133312447935, 2012.

615 Sultan, B., & Janicot, S.: The West African monsoon dynamics. Part II: The "preonset" and "onset" of the summer
616   monsoon. Journal of climate, 16(21), 3407-3427, https://doi.org/10.1175/1520-
617   0442(2003)016<3407:TWAMDP>2.0.CO;2, 2003.

618 Talib, J., Taylor, C. M., Klein, C., Harris, B. L., Anderson, S. R. and Semeena, V. S.: The sensitivity of the West
619   African monsoon circulation to intraseasonal soil moisture feedbacks, Q. J. R. Meteorol. Soc., 148(745),
620   1709–1730, doi:10.1002/qj.4274, 2022.

621 Taylor, C.M., Belušić, D., Guichard, F., Parker, D.J., Vischel, T., Bock, O., Harris, P.P., Janicot, S., Klein, C. and
622   Panthou, G.: Frequency of Extreme Sahelian Storms Tripled since 1982 in Satellite Observations, Nature 544,
623   475-78, https://doi.org/10.1038/nature22069, 2017.

624 Thorncroft, C. D., Nguyen, H., Zhang, C. and Peyrille, P.: Annual cycle of the West African monsoon: Regional
625   circulations and associated water vapour transport, Q. J. R. Meteorol. Soc., 137(654), 129–147,
626   https://doi:10.1002/qj.728, 2011.

627 Vizy, E.K. and Cook, K.H.: Mesoscale Convective Systems and Nocturnal Rainfall over the West African Sahel:
628   Role of the Inter-Tropical Front, Clim. Dyn. 50, 587-614, https://doi.org/10.1007/s00382-009-0553-4, 2018.

629 Wolski, P., Jack, C., Tadross, M., van Aardenne, L. and Lennard, C.: Interannual Rainfall Variability and SOM-
630   Based Circulation Classification", Clim. Dyn. 50, 479-92, https://doi/org/10.1007/s00382 -017-3621-1, 2018.
631